

Bridging the Sensitivity Gap in Precipitation Estimates from Spaceborne Radars using Passive Microwave Observations

Simon Pfreunds Schuh,^a Christian D. Kummerow,^a

^a *Department of Atmospheric Science, Colorado State University, Fort Collins, USA*

arXiv:2604.23745v2 [physics.ao-ph] 8 May 2026

Corresponding author: Simon Pfreunds Schuh, simon.pfreunds Schuh@colostate.edu

ABSTRACT: Current global precipitation estimates from spaceborne precipitation radars are limited by their sensitivity to light and frozen precipitation, leading to systematic underestimation of precipitation at high latitudes. Because passive microwave retrievals are commonly trained using these radar observations as reference data, this limitation is propagated into passive microwave precipitation products.

This study introduces a novel passive microwave oceanic precipitation retrieval, GPROF-NN eXtended Precipitation Regime (XPR), that combines reference estimates from a cloud radar and a precipitation radar to overcome the sensitivity limitations of current spaceborne precipitation radars. The retrieval is trained to estimate light precipitation from CloudSat observations and moderate-to-heavy precipitation using observations from the GPM Dual-Frequency Precipitation Radar. The two estimates are combined using a fusion scheme to obtain a consistent precipitation estimate across precipitation regimes. Validation against in situ measurements from shipborne disdrometers shows a 26% improvement in the detection skill for high-latitude precipitation in terms of the critical success index and a reduction in the underestimation of high-latitude and frozen precipitation by more than 50% compared to retrievals constrained only by precipitation radar data. However, the fused retrieval does not improve the precision of instantaneous precipitation estimates, which is likely due to significant random errors in the CloudSat-based reference estimates of liquid precipitation.

These results demonstrate that passive-microwave retrievals can leverage the complementary sensitivities of cloud and precipitation radars to provide more consistent precipitation estimates across precipitation regimes than either reference instrument alone. The proposed retrieval provides a pathway to improve the representation of oceanic precipitation in future GPM precipitation products.

SIGNIFICANCE STATEMENT: Current satellite-based precipitation datasets underestimate high-latitude oceanic precipitation because the radar observations they are based on are insensitive to light and frozen precipitation. We address this issue by developing a novel precipitation estimation algorithm that uses passive microwave observations to estimate precipitation based on reference data from two different types of spaceborne radars: a cloud radar sensitive to light precipitation and a precipitation radar sensitive to moderate to heavy precipitation. This novel approach significantly improves precipitation detection capability and reduces systematic underestimation of oceanic precipitation at high latitudes, which we show by extensive validation against independent precipitation measurements from shipborne instruments. While the results demonstrate that global precipitation estimates of oceanic precipitation can be improved by leveraging the complementary observation capabilities of cloud and precipitation radars, additional analysis of the radar based estimates also reveals inconsistencies between precipitation estimates from the two radars highlighting remaining shortcomings precipitation estimates from spaceborne radars.

The algorithm developed in this work will be used to fill in missing light and frozen precipitation in the next version of passive microwave precipitation datasets from NASA's Global Precipitation Measurements mission. It presents an important step towards improved observations of the hydrological cycle at high latitudes.

1. Introduction

Precipitation is an important atmospheric process critical for sustaining terrestrial ecosystems and affecting a wide range of societal and economic activities. Measuring the global distribution of precipitation and its variability is an important prerequisite towards understanding – and, ultimately, predicting – the occurrence and intensity of precipitation. Satellite remote sensing is the principal technique for monitoring the global distribution of precipitation and therefore an essential tool for advancing the understanding of the global hydrological cycle.

However, even after three decades of dedicated satellite missions and scientific efforts to measure global precipitation, oceanic precipitation at high latitudes still remains poorly constrained. To illustrate this, Fig. 1 shows zonal means of oceanic precipitation from three principal precipitation datasets: passive microwave (PMW) precipitation estimates from GPM Microwave Imager (GMI) retrieved using V07 of the Goddard Profiling Algorithm (GPROF, Kummerow et al. (2015))

retrieval algorithm, the Global Precipitation Climatology Project (GPCP, Huffman et al. (2023)), and the ERA5 reanalysis (Hersbach et al. 2020). While the datasets are largely consistent across the tropics and mid-latitudes, the zonal means diverge poleward of 40 ° showing deviations of up to 80 % in the mid and high latitudes.

These large differences are due to a number of challenges. Light and frozen precipitation (< 0.1 mm/hr) contribute relatively more to total precipitation accumulations at high latitudes than in the tropics (Milani and Kidd 2023), and are harder to simulate in models due to weaker linkages to synoptic forcings. Light and frozen precipitation are also harder to estimate from satellite observations due to their weaker radiometric signatures (Kidd and Huffman 2011) and larger dependence on microphysical variations (Ekelund et al. 2020). In addition to this, current PMW retrieval algorithms such as GPROF are constructed to reproduce reference precipitation from the GPM Dual-Frequency Precipitation Radar (DPR). The limited sensitivity of the DPR causes these reference precipitation estimates to miss shallow and frozen precipitation and this behavior is in turn reproduced by the PMW retrieval algorithms based on the DPR reference estimates.

The CloudSat Cloud Profiling Radar (CPR, Stephens et al. (2008)) is a different spaceborne radar designed primarily to observe clouds. It operates at a frequency of 94.05 GHz, which makes it more sensitive to light precipitation and snowfall. The higher sensitivity, its higher spatial resolution and lower surface clutter height significantly improve its capability to detect precipitation compared to the DPR. However, the observations are also heavily attenuated by liquid precipitation, which complicates deriving quantitative precipitation estimates particularly for moderate and heavy precipitation.

Merged precipitation products such as the Integrated Multi-Satellite Retrieval for the Global Precipitation Measurement Mission (IMERG, Huffman et al. (2020)) and GPCP that rely on PMW retrievals compensate for the inherited insensitivity to light and frozen precipitation using climatological adjustments. GPCP, for example, rescales microwave retrievals using precipitation climatologies derived in part from the CPR, which allows extending reference observations to higher latitudes in addition to providing higher sensitivity to light and frozen precipitation. However, such corrections constrain long-term means rather than instantaneous retrievals and may therefore misrepresent the temporal variability of high-latitude precipitation.

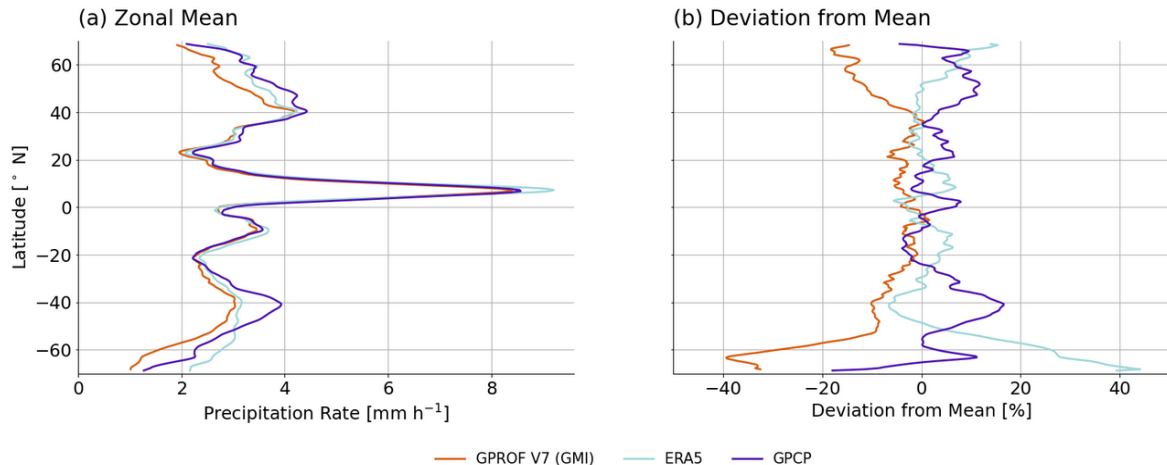


FIG. 1. Zonal means of oceanic precipitation from GMI, the GPCP merged precipitation dataset, and the ERA5 reanalysis. Panel (a) shows absolute precipitation rates; Panel (b) shows relative deviations from the cross-dataset mean.

Recent neural-network precipitation retrievals (Pfreundschuh et al. 2024) have improved performance across many regimes and are being adopted operationally. However, machine-learning retrievals approximate the conditional expectation defined by their training data and thus reproduce biases present in the reference observations. Training solely on DPR-based precipitation therefore propagates the radar’s limited sensitivity to light and frozen precipitation into the learned retrieval, regardless of retrieval technique used.

Here we aim to overcome the limitations of current DPR-based precipitation estimates by using PMW observations to bridge the sensitivity gap between the CPR and DPR precipitation estimates and thus achieve more complete representation of precipitation across regimes. Specifically, we propose GPROF-NN eXtended Precipitation Regime (XPR), a GMI-based retrieval that jointly predicts precipitation estimates based on CPR- and DPR-based reference precipitation rates. Since the CPR operates at a higher frequency, it is more sensitive to small and frozen hydrometeors and can thus be expected to provide a better representation of light and frozen precipitation. DPR, on the other hand, misses light and frozen precipitation but provides reliable estimates of moderate and heavy precipitation. The GPROF-NN XPR retrieval is trained to map GMI PMW observations to both a light precipitation estimate based on CPR reference data and an estimate of moderate to heavy precipitation based on DPR reference data. As we will show here, an improved representation of precipitation across regimes can be obtained by using the CPR-based precipitation estimates to fill in missing light precipitation in the DPR-based Estimates.

GPROF-NN XPR has been developed as an auxiliary retrieval to recover missing oceanic precipitation in DPR-based reference data used by previous versions of the GPROF and GPROF-NN (Pfreundschuh et al. 2022) retrievals. It is part of the development of GPROF V08 – the next operational version of the GPM PMW retrievals – and aims to address the systematic underestimation of high latitude precipitation. The previous operational version of GPROF – GPROF V07 – used light precipitation estimates from the MiRS algorithm (Boukabara et al. 2011) to fill in missing precipitation in DPR estimates but this was unsuccessful in fully addressing the underestimation. The filling in of missing oceanic precipitation complements several other interventions addressed to fix shortcomings in the DPR data used as a priori database and training dataset such as the use of ground-based radar estimates over snow-covered surface and the use of ERA5 precipitation over sea ice.

This manuscript describes the GPROF-NN XPR retrieval and validates its precipitation estimates using in-situ measurements from shipborne distrometers demonstrating its ability to improve the detection of light and frozen precipitation and reduce climatological biases. Additionally, we provide a validation of the CPR- and DPR-based reference estimates against independent measurements from ground-based precipitation radars. Section 2 describes the retrieval implementation as well as the data used to validate the retrievals. Section 3 assesses and validates the GPROF-NN XPR retrieval, validates the radar-based reference estimates, and assesses the effect of the enhanced sensitivity of the GPROF-NN XPR retrieval on the climatological precipitation distribution. Finally, section 4 summarizes and discusses the main findings from this work.

2. Methods and Data

The GPROF-NN XPR retrieval algorithm is a machine-learning based precipitation retrieval that is trained to simultaneously provide estimates of CPR-based and DPR-based precipitation rates. The two estimates are subsequently fused to provide a general precipitation estimate that better represents precipitation across the full spectrum of intensities. Below we describe the retrieval implementation together with the data sources used to validate the retrieval itself as well as the two radar-based reference datasets.

a. The GPROF-NN XPR Retrieval

The GPROF-NN XPR retrieval is based on the GPROF-NN retrieval framework introduced in (Pfreunds Schuh et al. 2022) and subsequently validated in (Pfreunds Schuh et al. 2024). It uses the same neural-network architecture as the upcoming version of GPROF-NN, which is currently under development and will become the operational precipitation retrieval of the GPM constellation as GPROF V08.

NEURAL NETWORK MODEL

The GPROF-NN XPR retrieval employs a U-Net–type encoder–decoder architecture composed of EfficientNet-V2–style inverted bottleneck convolutional blocks (Tan and Le 2021). Following the normalization and activation design adopted in ConvNeXt (Liu et al. 2022), each convolutional block uses Layer Normalization (Ba et al. 2016) and GELU activation functions (Hendrycks and Gimpel 2016). The network input consists of GMI brightness temperatures together with the corresponding earth-incidence angles (EIA) for all channels and a set of ancillary variables. These ancillary data describe both surface conditions (land fraction, elevation, mountain classification, leaf-area index, ice fraction, and snow depth) and the meteorological environment (2-m temperature, 10-m wind speed, orographic wind, and total column water vapor).

The model produces two precipitation estimates: one trained on CPR-based reference precipitation and one trained on DPR-based reference precipitation. Both estimates are derived from a shared latent representation using separate multilayer perceptron output heads. Each head predicts 32 quantiles of the conditional precipitation distribution, which are learned using quantile regression (Pfreunds Schuh et al. 2018). The expectation is that the CPR-based reference data will miss heavy rain where CPR is attenuated while the DPR-based reference will miss light precipitation below the detection threshold of those radars.

TRAINING DATA AND TRAINING

The training dataset for the GPROF-NN XPR retrieval is constructed from two independent sets of collocations between GMI observations and reference precipitation estimates from the CPR and DPR sensors.

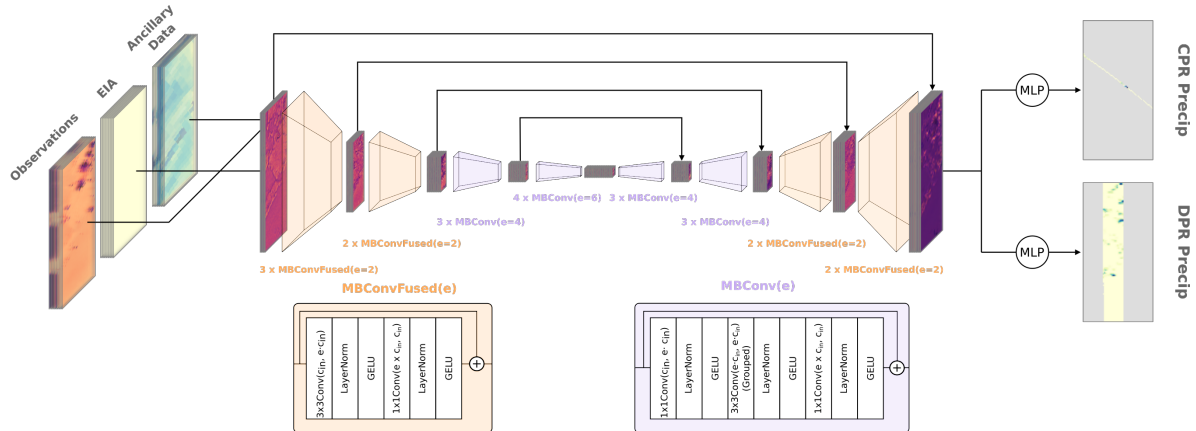


FIG. 2. Illustration of the U-Net neural network used by GPROF-NN XPR. The network employs MobileNet convolutional blocks (MBConv) within an encoder–decoder architecture. Input features consist of image patches of GMI brightness temperatures, corresponding earth-incidence angles (EIA), and ancillary variables. These inputs are mapped to a shared latent representation from which two precipitation estimates are derived through separate output heads: a CPR-based light precipitation estimate and a DPR-constrained moderate-to-heavy precipitation estimate.

For the GMI–CPR dataset, precipitation estimates are derived by combining information from the 2C-Precip-Column (Haynes et al. 2009), 2C-Rain-Profile (Lebsock and L’Ecuyer 2011), and 2C-Snow-Profile (Wood et al. 2014) products. Precipitation rates are assigned according to the precipitation classification in 2C-Precip-Column: pixels flagged as non-precipitating are assigned zero precipitation; pixels classified as certain rain are assigned the rate from 2C-Rain-Profile; pixels classified as certain snow are assigned the rate from 2C-SnowProfile. Pixels that do not meet any of these conditions or are assigned a retrieval confidence less than three are treated as missing and excluded from training. The dataset includes all GMI-CPR collocations from 2014–2017 with a maximum temporal separation of 15 min between the GMI and CPR observations. Collocations from January–October 2018 are used for validation, and those from October 2018–October 2019 are reserved for testing.

For the GMI–DPR dataset, precipitation rates are taken from the GPM 2BCMB (Grecu et al. 2016) combined radar–radiometer product. Because GMI and DPR observe from the same platform, these collocations are substantially more numerous than the GMI–CPR matchups. During training, the GMI–CPR samples are therefore oversampled such that, on average, every second training sample originates from the GMI–CPR dataset, ensuring similar representation of both reference regimes. The training is performed across 120 epochs using a cosine-annealing learning-rate schedule with an initial learning rate of 0.0005 and warm restarts after 20 and 60 epochs.

FUSED PRECIPITATION ESTIMATES

The GPROF-NN XPR retrieval produces a CPR-based and a DPR-based precipitation estimate for each GMI pixel. To provide a single precipitation estimate that properly describes precipitation across precipitation regimes, the two estimates must be combined. The fused precipitation relies on the CPR-based estimate when the DPR-based retrieval indicates no precipitation (reflectivities below the DPR threshold) and transitions to the DPR-based estimate as intensity increases (reflectivities likely attenuated in CPR). A simple linear transition, however, was found to introduce a notable artifact in the distribution of the fused precipitation rates. Instead, a zero-centered Gaussian weighting function was applied to obtain a smooth precipitation-rate distribution. The Gaussian has a full width at half maximum of 0.45 mm h^{-1} , with the resulting weighting function as well as the distribution of test-data precipitation rates shown in Fig. 3.

The distribution of the fused precipitation estimates follows that of the CPR-based estimates at low precipitation rates and transitions to follow the distribution of the DPR-based precipitation rates for moderate to high precipitation. The distribution of the GPROF-NN CPR precipitation estimates exhibits several irregularities and is less smooth than that of the GPROF-NN DPR estimates. We suspect that this may be related to the bimodal distribution of the 2C-Rain-Profile estimates that was noted already in Lebsock (2011). While the bulges in the PDF of GPROF-NN CPR precipitation estimates do not match the exact peaks of the distribution in Fig. 7 in Lebsock (2011), they may be shifted in the retrieved distributions due to the increased resolution of the GMI-based GPROF-NN retrievals.

b. Validation Data

We validate both the GPROF-NN XPR retrieval and the underlying CPR- and DPR-based precipitation estimates using independent observations. The GMI-based GPROF-NN XPR estimates are validated against in situ measurements from shipborne disdrometers, which provide the most direct reference data available for oceanic precipitation. Owing to the much narrower swaths of the DPR and CPR, there are not enough overpasses to meaningfully evaluate the radar-based reference estimates with the shipborne measurements. Instead, their consistency is assessed using overpasses along the U.S. East Coast, where the satellite estimates are compared with coincident observations from ground-based weather radars.

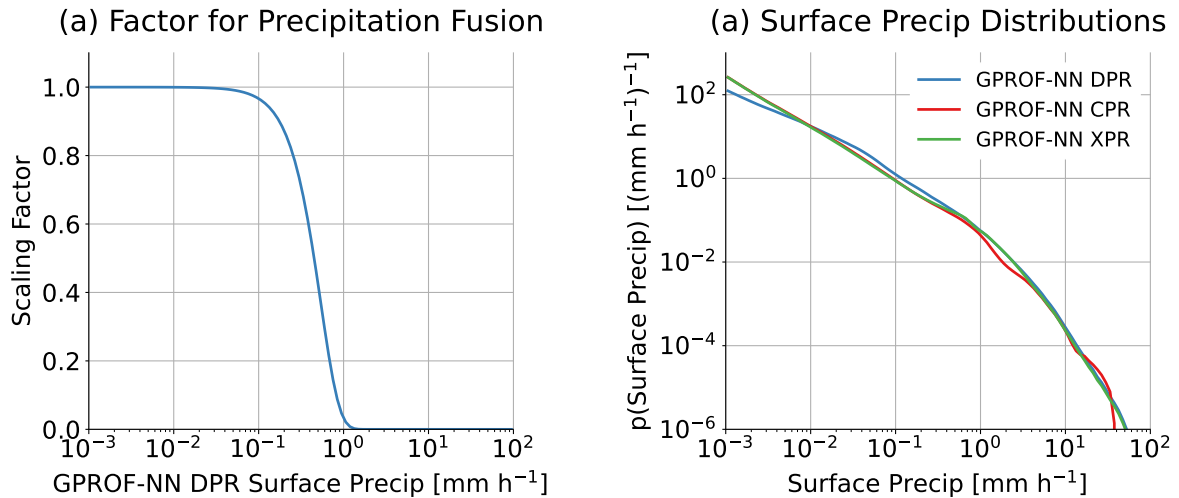


FIG. 3. Scaling factors used to fuse CPR- and DPR-based precipitation estimates (a) and resulting precipitation rate distributions (b).

OCEANRAIN SHIP-BASED DISTROMETER MEASUREMENTS

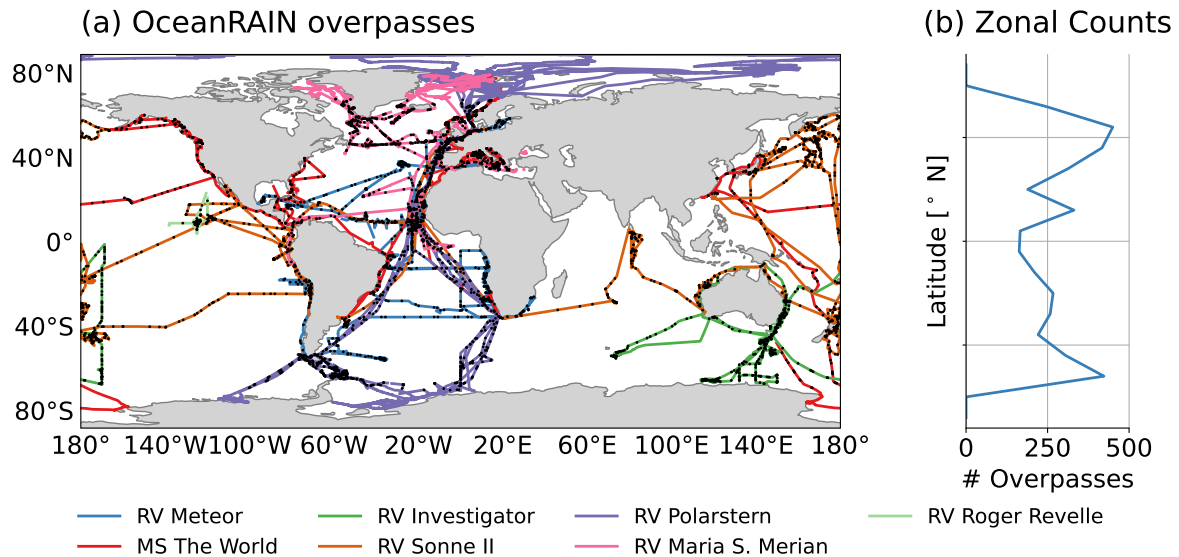


FIG. 4. OceanRAIN ship tracks and corresponding GMI overpasses. Colored lines indicate the trajectories of OceanRAIN vessels during the GMI observation period, and black dots denote the collocated satellite overpasses used for validation of the GPROF-NN XPR retrieval.

The OceanRAIN dataset (Klepp et al. 2018) provides shipborne disdrometer measurements of precipitation rates over the ocean. For validation of the GPROF-NN XPR retrieval, we identify GMI overpasses of the ship locations from March 2014, the start of GMI observations, through September 2018, prior to the period used to extract GPM–DPR training collocations. Because

this interval overlaps with the GMI–CPR training dataset, 64 matchups coinciding with CloudSat overpasses were excluded from the validation dataset.

Figure 4 shows the ship tracks associated with the OceanRAIN campaigns together with the corresponding GMI overpasses. To account for the spatial scale mismatch between satellite footprints and the distrometer measurements, the satellite estimates are compared with 30-min rolling averages of the distrometer precipitation rates. The matched satellite precipitation is computed by computing the GMI pixel closest to the ship position for each minute in the averaging window and averaging the resulting precipitation estimates.

To eliminate the impact of errors in the validation data, a relative error is calculated using

$$\text{err} = \frac{|p_{\text{retrieved}} - p_{\text{reference}}|}{\max(0.5, 0.5 \cdot |p_{\text{retrieved}} + p_{\text{reference}}|)}. \quad (1)$$

The error is calculated for the GPROF-NN DPR retrieval as well as the corresponding GPROF V07 and ERA5 precipitation estimates. Samples where the minimum relative error across these three datasets exceeds 1.8 are discarded. In total, 26 samples from the 3436 collocations with valid precipitation estimates fail to meet this quality criterion. The removed overpasses correspond to precipitation events missed by the distrometer as well as cases where the distrometer indicates very high precipitation rates not seen in the satellite or ERA5 data. The exclusion of these events does not impact the qualitative results of the validation.

GROUND-BASED PRECIPITATION RADAR ESTIMATES

To provide additional context for the evaluation of the GPROF-NN XPR retrieval, we assess the CPR and DPR reference precipitation estimates using independent observations from NOAA’s Multi-Radar Multi-Sensor (MRMS, Smith et al. (2016)) product along the U.S. East Coast. For the CPR-based estimates, all available overpasses from June 2015 through the end of the CloudSat mission are included. Owing to the wider swath of the DPR, overpasses from the year 2022 alone provide sufficient sampling for a robust comparison.

Because this study focuses on oceanic precipitation, only satellite pixels located over the ocean are retained. Since the chance for beam overshoot increases with distance from the shore, only MRMS pixels with a radar quality index (RQI) exceeding 0.9 are retained, limiting the distance

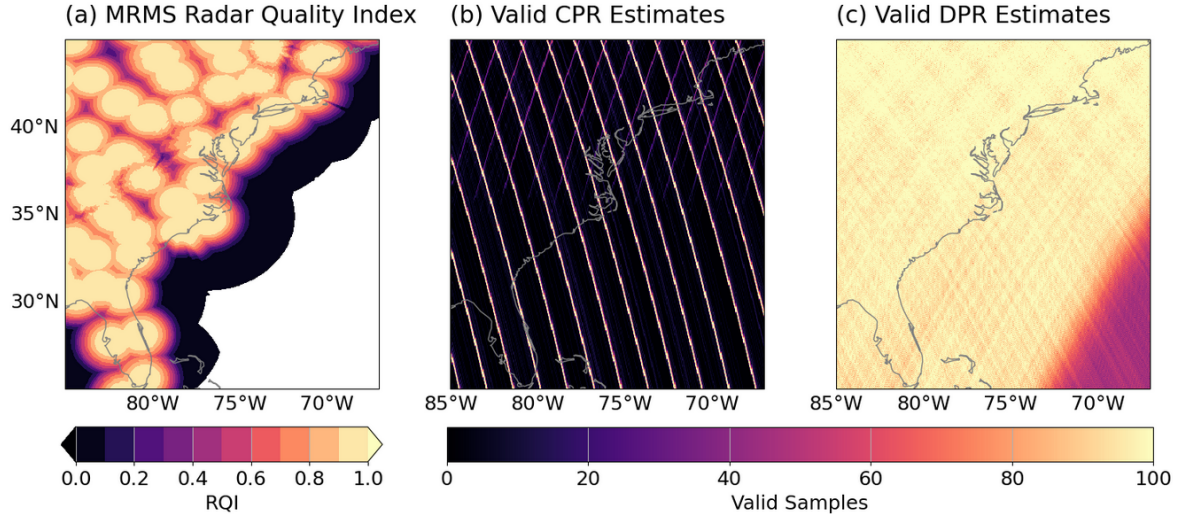


FIG. 5. Summary statistics the validation data derived from NOAA’s Multi-Radar Multi-Sensor data. Panel (a) shows the radar-quality index quantifying the quality of the radar measurements. Panel (b) and (c) show the mean precipitation and precipitation occurrence, respectively.

to the closest radar to about 100 km. As RQI fields are unavailable for some earlier MRMS periods, the mean RQI field from 2022 is used to screen the matched observations. Following (Pfreundschuh et al. 2026), the MRMS precipitation fields are aggregated to a $0.36^\circ \times 0.36^\circ$ grid and collocated with the CloudSat and DPR estimates using nearest-neighbor interpolation. Panel (a) of Fig. 5 presents the mean radar quality index (RQI) used to filter valid match-ups. Even with a minimum RQI threshold of 0.9, the NEXRAD network provides coverage across most of the U.S. East Coast. Panels (b) and (c) display the total number of valid precipitation retrievals extracted within the validation domain before the RQI mask is applied. Valid CloudSat retrievals are largely limited to ascending overpasses due to its restriction to daytime-only operation during the validation period. A smaller number of descending overpasses are available over the northern portion of the domain during summer. In contrast, the substantially wider swath of the DPR results in far more frequent observations that are distributed more uniformly across the domain.

3. Results

Below we present the three principal results from this work: Firstly, we assess the accuracy of the GPROF-NN XPR retrieval by comparing it to GPM CMB and CloudSat estimates from independent testing periods and a case study from the validation period. Following this, we

validate the fused GPROF-NN XPR retrieval as well as CPR- and DPR-based precipitation estimates against independent in-situ precipitation estimates. Finally, we compare global retrieval statistics to existing datasets to assess the impact of the expanded reference data on the GPROF-NN XPR retrievals.

a. Retrieval Accuracy

Figure 6 shows scatter plots of reference and retrieved precipitation rates for the CPR- and DPR-based outputs of the GPROF-NN XPR retrieval. The retrieval reproduces the DPR-based estimates well, achieving low bias and mean-squared error and high linear correlation. The accuracy of the CPR-based estimates is substantially lower: MSE and correlation coefficient indicate lower accuracy that is also reflected in the increased spread of the retrieved values. In part, this can be explained by the higher resolution of the CPR-based precipitation estimates. The training and testing datasets both use CPR estimates at the native resolution (1.6 km), whereas the DPR-based estimates are downsampled to the GMI resolution, which is how they are traditionally treated in the GPROF framework. The different approach for the CPR-based estimates was chosen due to the difficulties of assigning a unique resolution to the GMI observations and of matching the one-dimensional CPR data to the two-dimensional GMI footprints.

The CPR-based precipitation estimates show fair agreement with the reference values from 0.1 to 3–4 mm h⁻¹ but struggle to reproduce precipitation estimates exceeding that. However, since CloudSat estimates have to be considered very uncertain in this range, it is possible that this is – at least in part – due to errors in the CPR-based reference data. Additionally, there is a notable bias in the CPR-based precipitation estimates of about 13% which is caused by the underestimation of the higher rain rates. Given that precipitation rates exceeding 3–4 mm/h account for more than 10 % of the total precipitation in the test data, the bias may be caused by statistical fluctuations and the smaller number of testing samples compared to the DPR-based estimates. Furthermore, since CloudSat left the A-train in 2018, the precipitation estimates from the test data were derived in a different orbital configuration, which can further affect bulk precipitation statistics and thus produce biases in the test results.

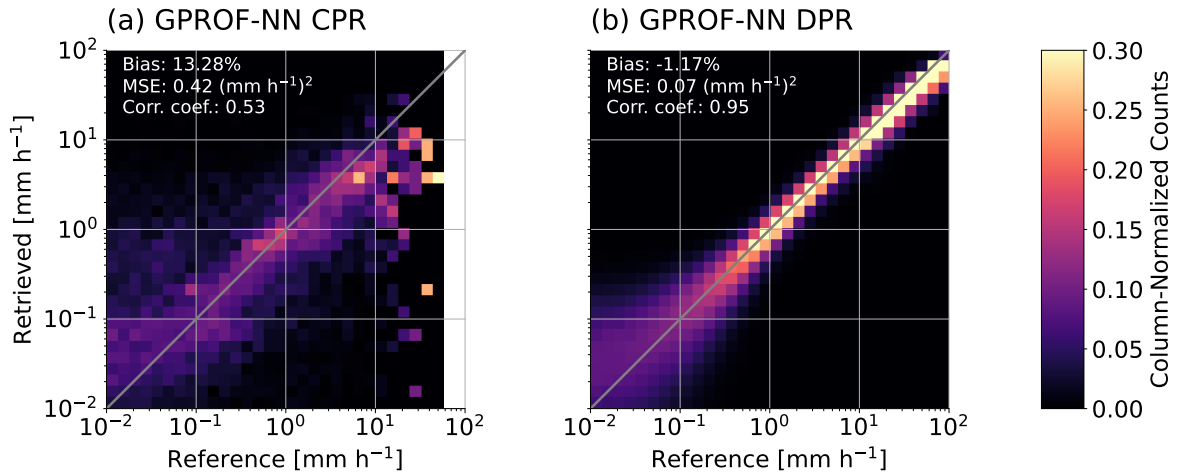


FIG. 6. Scatter plots of reference and retrieved precipitation for the (a) CPR-based and (b) the DPR-based precipitation estimates.

b. Case Study

Figure 7 illustrates an example of the DPR- and CPR-based precipitation estimates together with the resulting fused estimate. The case study displays a GMI overpass of a Southern Hemisphere mid-latitude cyclone in June 2018. A comparison of the CPR-based, DPR-based, and fused XPR precipitation fields highlights substantial structural differences among the three products. Although the CPR- and DPR-based estimates are generated using the same model, they exhibit marked discrepancies. The CPR-based retrieval produces higher precipitation intensities and a broader spatial extent of the cyclone’s precipitation field. The fused XPR product moderates the elevated precipitation rates evident in the CPR-based retrieval while largely preserving its enhanced spatial coverage.

Comparison with the reference data along the CloudSat swath shows that the GPROF-NN XPR retrieval successfully captures the shallow precipitation occurring between 200 and 250 km along the CloudSat track that is missed by both the DPR reference estimates and the GPROF-NN DPR retrievals. Generally, the GPROF-NN XPR results capture the main precipitation features but do not reproduce the small-scale variability present in the radar-based reference estimates. This discrepancy is expected because PMW observations have coarser spatial resolution and sampling than the radar measurements. At around 50 km and 750 km along the swath, the GPROF-NN XPR retrieval indicates precipitation while the CPR-based estimates suggest little or no precipitation. However, the CPR radar still detects reflectivities extending down to the surface in these regions,

suggesting that precipitation likely reaches the surface but may be overestimated by the PMW retrieval.

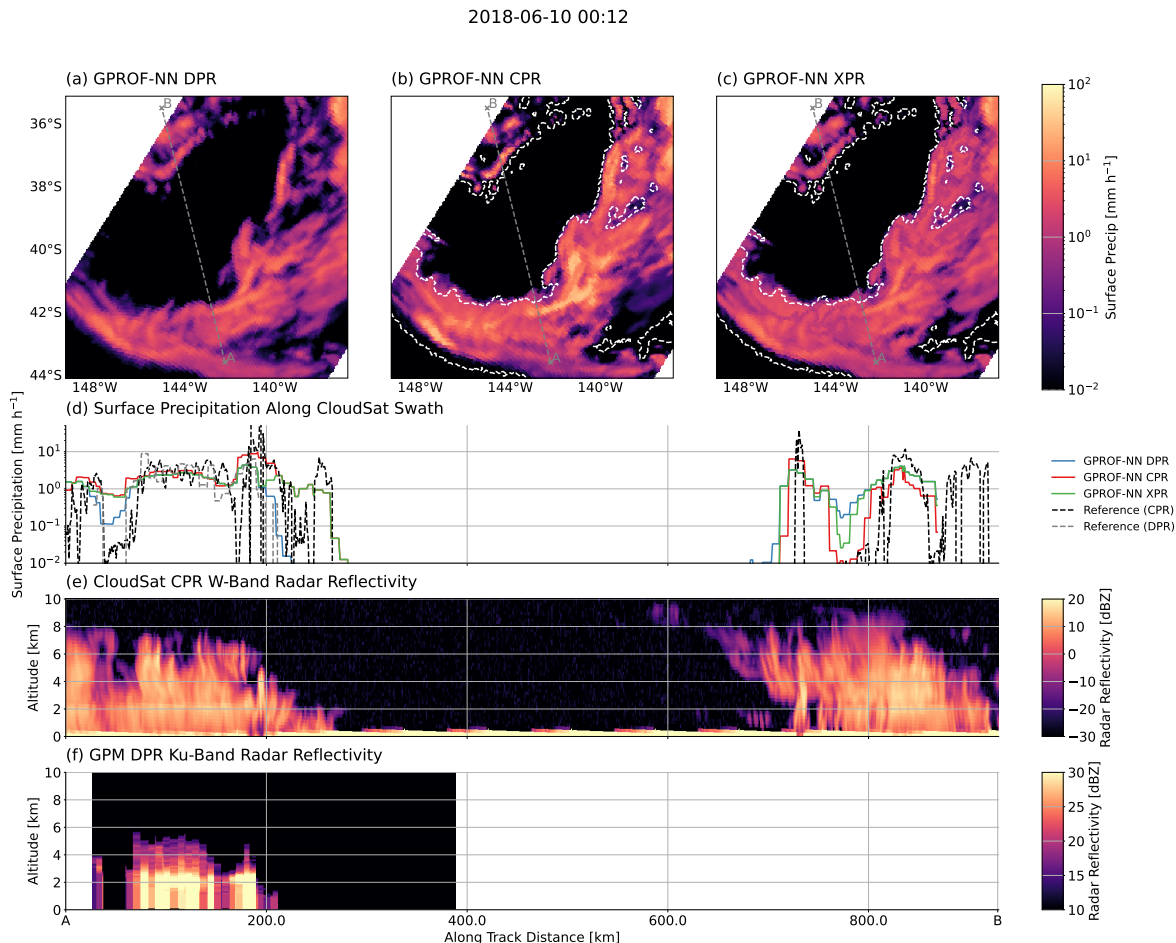


FIG. 7. Coincident observations of a mid-latitude cyclone by the GPM and CloudSat satellites. The first row of panels displays GMI-based PMW retrievals trained on GPM DPR precipitation (a), on CloudSat CPR precipitation (b), and the fused precipitation field combining the DPR- and CPR-based estimates (c). Panels (d), (e), and (f) show the retrieved precipitation and the corresponding CloudSat and GPM radar reflectivities along the CloudSat swath.

c. Validation

The results presented above demonstrate that the GPROF-NN XPR retrieval is able to reproduce both CPR- and DPR-based precipitation estimates accurately considering the differences in resolution and information content of the PMW observations as well as the sensitivity ranges of the two reference datasets. However, since neither reference dataset accurately captures precipitation accurately across the full spectrum of precipitation intensities, it is essential to evaluate the GPROF-NN

XPR retrieval against independent precipitation measurements to ensure it actually improves the representation of precipitation. Below we validate both the GPROF-NN XPR retrieval as well as the reference datasets themselves against independent precipitation measurements.

1) OCEANRAIN

The GPROF-NN XPR precipitation estimates are evaluated using 3410 OceanRAIN overpasses that passed quality control and yielded valid precipitation estimates from GPROF V07, ERA5, and GPROF-NN XPR. To provide a more granular assessment, we stratify the analysis into three subsets: (1) all overpasses, (2) high-latitude cases poleward of 45° , and (3) scenes with a high likelihood of mixed or frozen precipitation. The latter classification uses the parameterization of Sims and Liu (2015) with ERA5-derived wet-bulb temperatures. Overpasses with a conditional probability of solid precipitation exceeding 50% are categorized as likely mixed or frozen precipitation events.

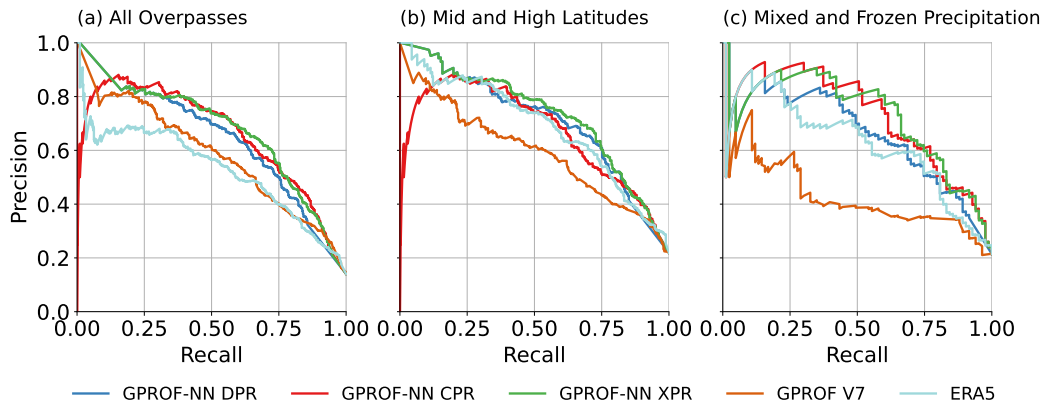


FIG. 8. Precipitation-detection skill evaluated against ship-borne distrometer measurements. Each panel shows precision–recall curves for the GPROF-NN XPR retrieval outputs based on CPR estimates (GPROF-NN CPR), the DPR-based precipitation estimates (GPROF-NN DPR), the fused estimates (GPROF-NN XPR) and the GPROF V07 and ERA5 baselines. c Panels (a) – (c) show precipitation estimates for all overpasses, overpasses for latitudes poleward of 45° , and for mixed and frozen precipitation, respectively.

(i) *Precipitation Detection* We first assess the detection capability of the three GPROF-NN retrievals as well as GPROF V07 and ERA5 baselines using precision-recall curves. The precision recall curves display the trade off between precision, i.e., the probability of a detection being correct, and the recall, i.e., the fraction of total precipitation events detected, as the probability threshold used to decide whether a pixel is raining or not is varied. The more skillful the detection,

the closer the curve gets to a precision and recall value of one. All GPROF retrievals provide a probability of precipitation representing the estimated probability of the corresponding pixel containing precipitation. Since ERA5 doesn't provide a dedicated probability field for precipitation occurrence, we use the precipitation rate as detection criterion. An overpass is defined to be precipitating when the half-hour average distrometer precipitation exceeds 0.01 mm/h.

Figure 8 displays the precipitation detection accuracy for all overpasses, overpasses at high latitudes, and mixed and frozen precipitation. Considering all overpasses, the CloudSat-based light precipitation and the fused GPROF-NN XPR results yield the highest detection accuracy. This is consistent with the CloudSat-based precipitation estimates providing higher sensitivity to light precipitation that is missed by the GPM DPR reference data. The retrieval based solely on GPM DPR data has slightly lower detection skill but remains clearly more sensitive than the GPROF V07 and ERA5 baselines.

Somewhat surprisingly, the detection accuracy of the DPR-based estimates exceeds that of the CPR-based estimates at mid and high latitudes. This seems to indicate that the CPR-based GPROF-NN estimates miss certain precipitation events that are detected by the DPR-based estimates but it is not immediately clear for which precipitation processes this would occur. The GPROF-NN XPR achieves the highest precipitation detection skill exceeding that of both the CPR- and the DPR-based retrievals.

Although the results for mixed and frozen precipitation are overall noisier, the CPR-based and fused precipitation estimates clearly achieve the best detection accuracy. The DPR-based retrieval performs worse and is closely followed by ERA5. The GPROF V07 retrieval performs substantially worse with the best precision and recall values being about half of the GPROF-NN XPR retrieval.

Table 1 evaluates the detection skill of all retrievals that provide a probability of precipitation using a probability threshold of 0.5. This evaluation confirms that the GPROF-NN XPR retrieval yields the best detection skill across all precipitation regimes. In particular, the GPROF-NN XPR retrieval improves the detection skill compared to GPROF-NN DPR by 48 %, 26 %, and 42 % for all overpasses, mid and high latitudes overpasses, and frozen precipitation, respectively.

(ii) *Precipitation Estimation* Figure 9 assesses the quantitative precipitation estimates of the GPROF-NN retrievals with respect to the OceanRAIN reference. The GPROF-NN DPR retrieval achieves higher correlation with the OceanRAIN measurements than the CPR-based estimates,

TABLE 1. Precipitation detection metrics (POD, FAR, CSI) for different retrieval methods evaluated against shipborne distrometer measurements across precipitation regimes.

Method	All Overpasses			Mid and High Latitudes			Frozen Precipitation		
	POD	FAR	CSI	POD	FAR	CSI	POD	FAR	CSI
GPROF V07	0.37	0.31	0.32	0.29	0.28	0.26	0.11	0.25	0.10
GPROF-NN DPR	0.85	0.65	0.33	0.85	0.56	0.41	0.90	0.63	0.36
GPROF-NN CPR	0.44	0.23	0.39	0.45	0.23	0.40	0.66	0.35	0.49
GPROF-NN XPR	0.67	0.35	0.49	0.65	0.28	0.52	0.71	0.36	0.51

which exhibit higher spread at both low- and high-precipitation rates. To assess the impact of the precipitation-rate fusion, panel (c) displays the relative change in the symmetric mean percentage error (SMAPE) resulting from the combining of the DPR- and CPR-based estimates compared to the DPR baseline. While the merging decreases the SMAPE for a significant number of samples ending up close to the diagonal, there are a notable amount of samples for which the SMAPE is increased. Most of these correspond to the merging leading to an overestimation of the precipitation. Since the coloring indicates the increase in the relative error, the largest increases in error occur at small reference precipitation rates as the relative error is more sensitive in these regimes. For a smaller number of red samples below the diagonal, the merging with the CPR estimates erroneously reduces the final precipitation rate.

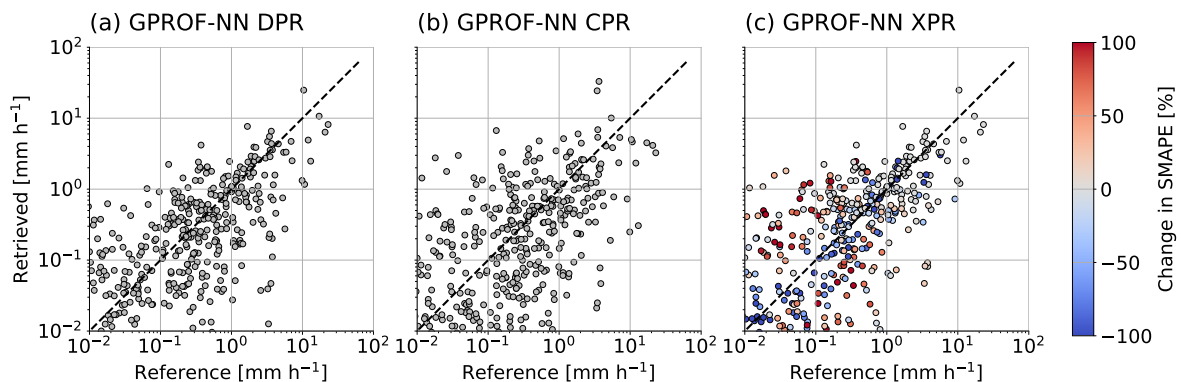


FIG. 9. OceanRAIN measurements and matches GPROF-NN precipitation retrievals. Panels (a) – (c) display scatter plots of OceanRAIN reference precipitation and corresponding precipitation retrieved from the GPROF-NN DPR, GPROF-NN CPR, and GPROF-NN XPR retrievals. Shading in panel (c) indicates the change in the Symmetric Mean Percentage Error resulting from the merging of the DPR- and CPR- based estimates relative to the GPROF-NN DPR baseline.

A statistical evaluation of the OceanRAIN overpasses is presented in Fig. 10. Evaluated over all overpasses, both the DPR- and CPR-based estimates are biased low. The bias of the DPR-based

estimates is around 10 %, while the DPR-based estimates are biased low by 7 %. Fusing the two estimates leads to a reduction in bias to a positive bias of about 1 %. At mid- and high latitudes, the low bias of the DPR estimates is enhanced while the CPR estimates are biased high with 16 %. The fused precipitation estimates are biased low by about 7 %. For frozen precipitation, the bias in the DPR-based estimates increases to 51 % while the CPR-based estimates are low by 20 %. The bias in the fused GPROF-NN XPR precipitation estimates is -20 %, similar to that of the CPR-based estimates. The fusion of the DPR- and CPR- based estimates thus helps to reduce systematic underestimation of the DPR-based retrieval. Furthermore, the biases are smaller than for the GPROF V07 baseline as well as the ERA5 baseline except for frozen precipitation.

In terms of instantaneous retrieval error, the CPR-based estimates have higher errors than the DPR-based estimates, particularly at mid to high latitudes. The fused estimates dampen these errors to some extent but remain higher or at the level of the DPR-based estimates. The GPROF-NN XPR retrieval generally achieves lower mean absolute and mean squared error than the ERA5 baseline as well as higher correlation. The GPROF V07 baseline has smaller mean squared error and higher correlation coefficient for all overpasses and higher correlation for frozen precipitation. However, comparing the GPROF estimates to the actual DPR-based reference estimates using the 1028 OceanRAIN overpasses with valid 2BCMB reference precipitation estimates, the GPROF-NN DPR estimates achieve a MSE of $0.26 \text{ (mm h}^{-1}\text{)}^2$ and a linear correlation coefficient of 0.84 compared to $0.32 \text{ (mm h}^{-1}\text{)}^2$ and a linear correlation of 0.8 for the GPROF V07 baseline. This indicates that these small accuracy differences are likely due to either statistical noise or uncertainties in the validation data.

2) VALIDATION OF CPR- AND DPR-BASED PRECIPITATION ESTIMATES

The validation against OceanRAIN shipborne distrometer measurements has shown that the fusion of CPR- and DPR-based precipitation estimates improves the precipitation detection skill and reduces systematic underestimation but increases the random errors in the precipitation estimates. Assessment of the CPR- and DPR-based estimates showed that these higher errors originate from the CPR-based estimates, which exhibit significantly larger random errors than the DPR-based estimates. Below we therefore examine CPR- and DPR-based precipitation errors against independent estimates from ground-based radars.

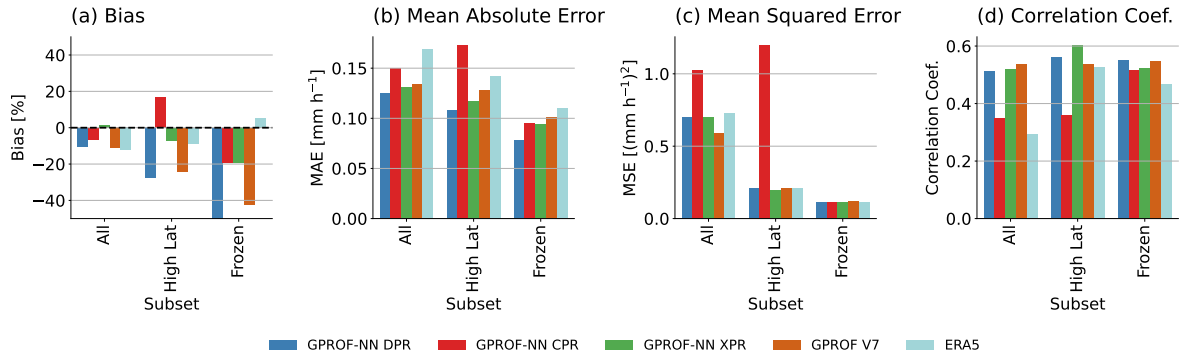


FIG. 10. Statistical evaluation of the GPROF-NN and baseline datasets against shipborne in-situ measurements from the OceanRAIN dataset. Panels (a) – (d) display bias, mean absolute error, mean squared error, and linear correlation coefficient for GMI overpasses over the OceanRAIN vessels. Results are reported independently for all overpasses (All), overpasses poleward of 45 deg (High Lat) and overpasses with an estimated fraction of frozen precipitation exceeding 50 % (Frozen).

Figure 11 displays scatter plots of the CPR- and DPR-based precipitation estimates compared to ground-based radar measurements of the US East Coast. The CPR-based precipitation estimates exhibit very high scatter compared to the MRMS-based measurements particularly for MRMS precipitation rates up to 1 mm/h. This is surprising given that the CloudSat estimates are expected to be more reliable at low precipitation rates, where the radar observations are less affected by attenuation. Nonetheless, the estimates achieve a correlation of 0.4 likely due to the better agreement for MRMS precipitation rates exceeding 1 mm h⁻¹. The scatter plot indicates a distinct bi-modal behavior for MRMS precipitation rates less than 1 mm h⁻¹, where the retrieval tends to either heavily overestimate or underestimate the MRMS precipitation rates but almost never matches them.

The DPR-based estimates show better agreement with the MRMS estimates. Although the DPR estimates strongly overestimate any MRMS estimates below 0.5 mm/h, which is a result of the limited sensitivity of the DPR, they show very good agreement with the MRMS-based estimates for precipitation rates from 5–10 mm/h, after which they start to exhibit a tendency towards under-estimation.

To illustrate the likely failure mode of the CPR precipitation retrievals, Figure 12 shows one of the CPR overpasses from the validation dataset. While the MRMS precipitation measurements indicate spatially homogeneous precipitation with precipitation rates around 1 mm h⁻¹ throughout

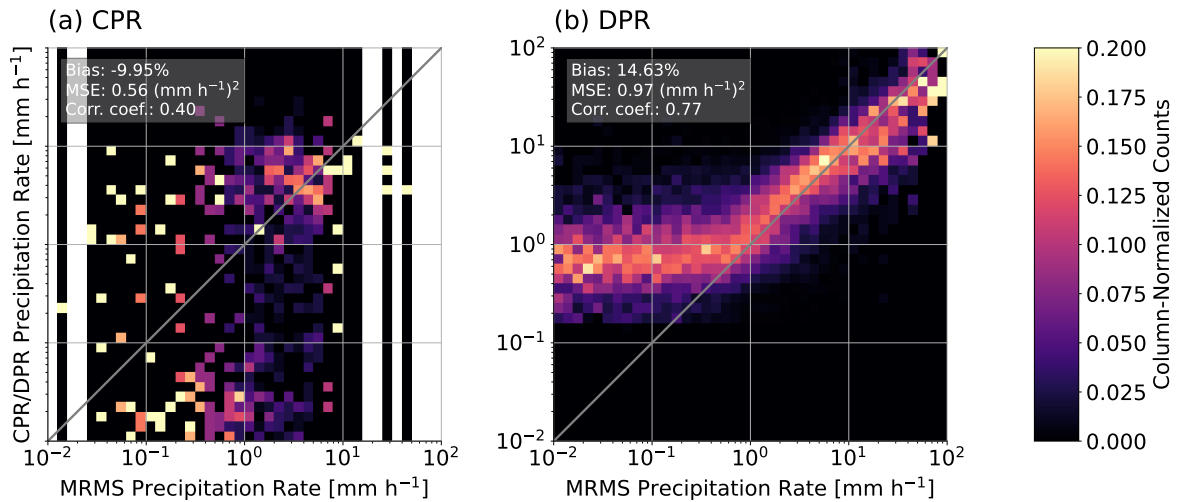


FIG. 11. Scatter plots of precipitation estimates from the (a) CPR- and (b) DPR-based reference precipitation estimates compared to independent estimates from ground-based radar.

most of the scene, the CPR-based precipitation oscillate between 0.01 and 10 mm h^{-1} . The principal change in CPR radar reflectivities during the transition from 10 mm h^{-1} to 0.01 mm h^{-1} is a strong increase in the surface backscatter while the above-surface reflectivities remain relatively similar. While limited, this evidence suggest that the errors in the CPR-based precipitation estimates may be related to the interpretation of the surface backscatter. Specifically in this scene where the surface backscatter increases, the estimate of the path integrated attenuation and column integrated precipitation water content decrease. One plausible source of uncertainty in this case is a localized change in the surface roughness not accounted for in the CloudSat algorithms.

The comparison against the independent precipitation estimates from MRMS indicates that the CPR-based precipitation estimates do not yield an accurate quantitative estimate of light precipitation. In particular, the retrieval seems to exhibit a tendency to either strongly underestimate or strongly overestimate MRMS precipitation rates within 0.1 to 1 mm/h . As shown in Fig. 13, this behavior is also observed when the CPR estimates are directly compared to the DPR-based estimates. Although one would expect the CPR and DPR estimates to agree across precipitation estimates from 0.5 to 1 mm h^{-1} , the scatter plot exhibits similar bi-modal behavior as for the validation against MRMS. The results in Fig. 11 further show that the inconsistency between the estimates is largely caused by the precipitation estimates from the 2C-Rain-Profile product. The snowfall estimates from the 2C-Snow-Profile product show generally better consistency particularly for estimates around 1 mm h^{-1} .

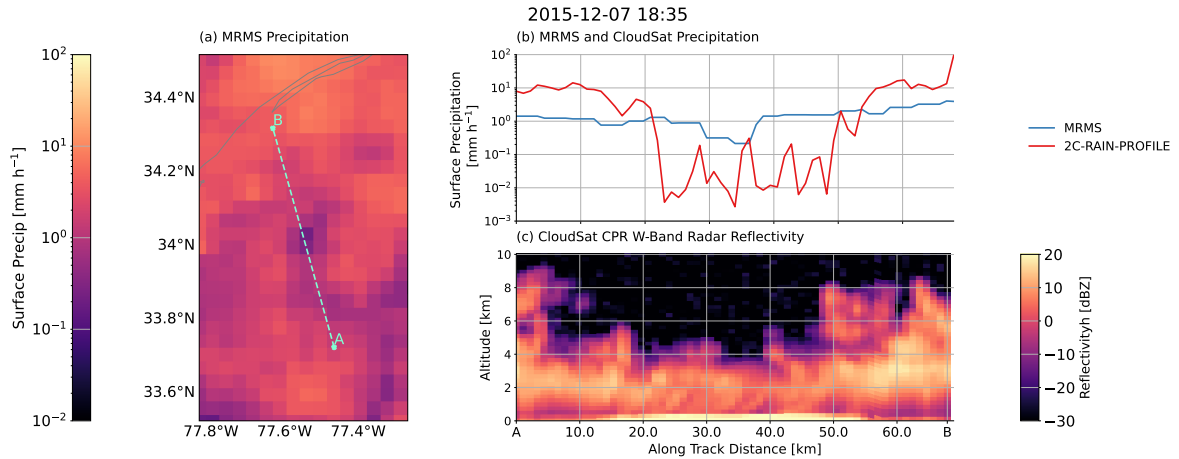


FIG. 12. Comparison of collocated CPR and MRMS precipitation estimates. Panel (a) displays the MRMS precipitation field and the ground track of the CPR observations. Panels (b) and (c) display the MRMS and CPR precipitation rates and the CPR radar reflectivity along the track, respectively.

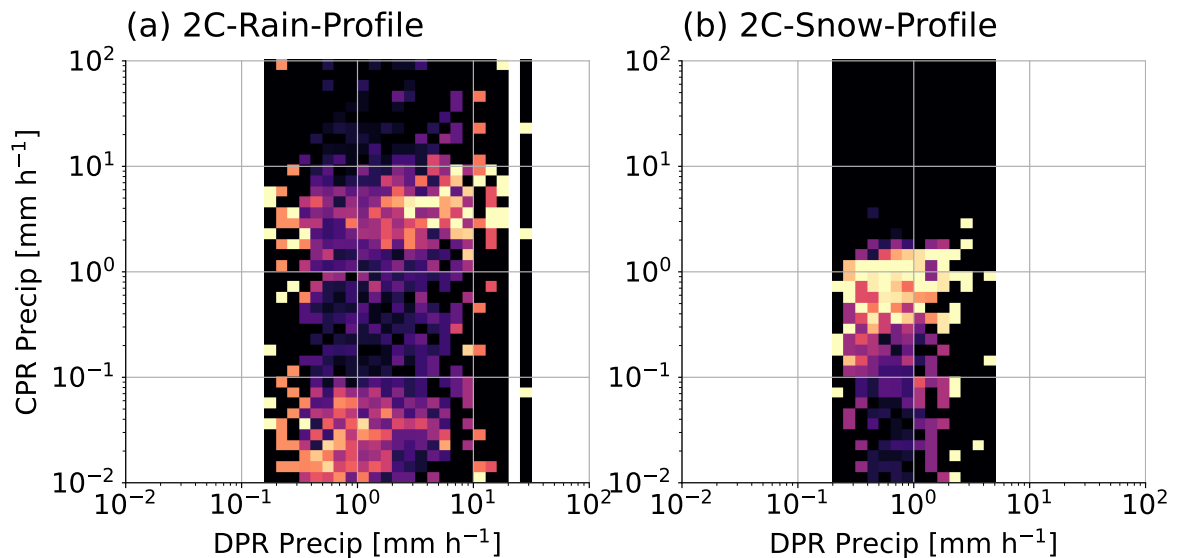


FIG. 13. Scatter plot comparing CPR- and DPR- based precipitation estimates. Panel (a) compares the DPR-based precipitation estimates from the GPM 2BCMB product with estimates of the CloudSat 2C-Rain-Profile product. Panel (b) compares the GPM estimates with snowfall estimates from the 2C-Snow-Profile product.

d. Global Precipitation Distributions

Although the fusing of CPR- and DPR- based precipitation estimates does not increase the accuracy of individual precipitation estimates, it has shown clear improvements in precipitation detection and reductions of climatological biases compared to shipborne distrometer measurements. This indicates that the fused GPROF-NN XPR estimates better represent light and frozen

precipitation. Below we characterize the impact of fusing CPR and DPR-based precipitation estimates on global precipitation distributions.

Figure 14 displays the zonal distribution of ocean precipitation as retrieved by the GPROF-NN CPR, DPR, and XPR retrievals. The CPR-based retrieval yields higher precipitation rates poleward of the mid-latitude storm tracks but severely underestimates precipitation in the tropics and extratropics compared to the estimates derived from DPR-based retrieval. The fused estimates track the GPM DPR-based estimates within 30° S – 30° N. Poleward of that, the GPROF-NN XPR estimates mostly fall between the DPR and CPR based estimates approximating the CPR-based estimates at high latitudes. The increased precipitation at mid and high latitudes moves the zonal profiles of the GPROF-NN XPR retrieval closer to those of of GPCP but remains lower than them at all latitudes. The GPROF-NN XPR retrieval is slightly higher than ERA5 in the storm tracks but falls below it at high latitudes.

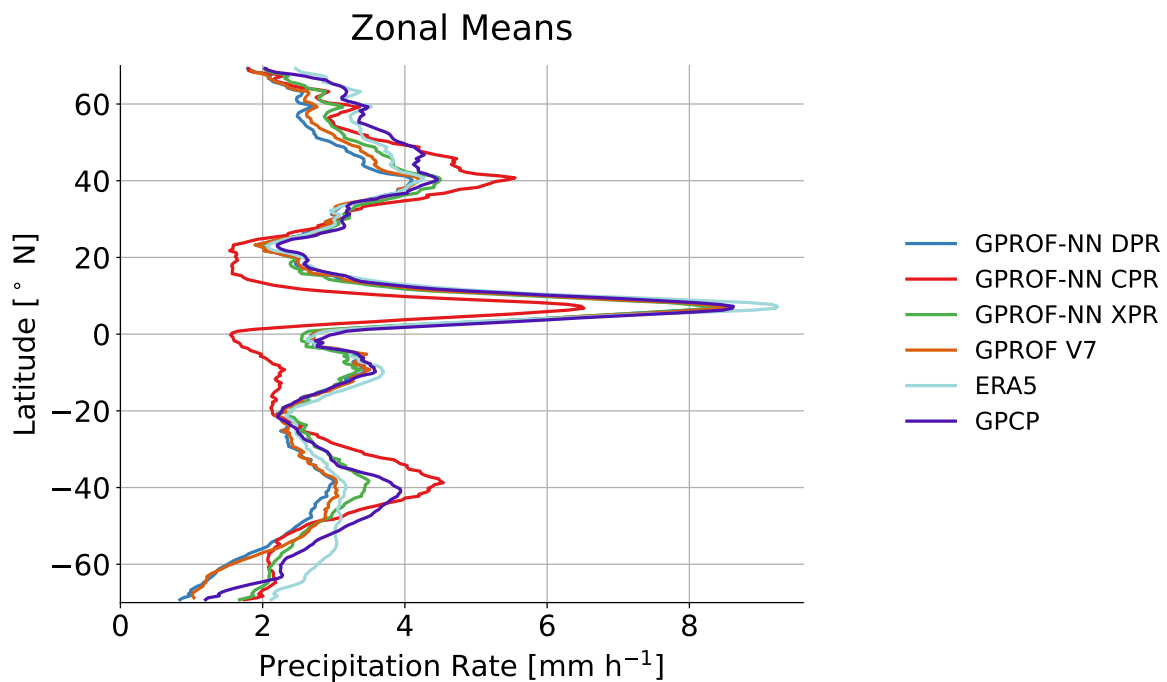


FIG. 14. Zonal means of oceanic precipitation estimates. The figure compares estimates from the CPR-based (GPROF-NN CPR), the DPR-based (GPROF-NN DPR), and from the fused precipitation estimates (GPROF-NN XPR) to reference estimates from GPROF V07, ERA5, and GPCP.

The corresponding global precipitation distributions are displayed in Fig. 15. Compared to the DPR-based retrievals, the CPR-based estimates add more than 2 mm per day over the storm tracks and high-latitude oceans. The fused XPR estimates add precipitation over the storm tracks and high

latitudes albeit less than the GPROF-NN CPR retrieval alone. The fused precipitation estimates slightly decrease precipitation over the Indian ocean and West Pacific but increase it over the eastern Pacific.

ERA5 exhibits higher precipitation rates than the DPR-based reference retrievals almost everywhere. However, pockets of decreasing precipitation are visible in the Indian Ocean and the West Pacific roughly matching areas of decreasing precipitation in the GPROF-NN XPR results. GPCP precipitation rates are also globally higher with scattered regions of decreasing precipitation.

Although the increased precipitation in the GPROF-NN XPR retrieval brings the zonal means closer to those of ERA5 and GPCP, the analysis of the global distribution highlights important differences between where the precipitation is added. In contrast to ERA5 and GPCP, the GPROF-NN XPR retrieval adds precipitation over the subtropical oceans off the west coasts of North and South America, Africa, and Australia. In addition to this, the GPROF-NN XPR slightly decreases precipitation over the tropical oceans east of the Americas. This may indicate that the fused retrieval is in fact sensitive to precipitation regimes that may be missed by the other datasets. However, given the inaccuracies in the CPR-based reference estimates, further validation is required to confirm this.

4. Summary and Conclusions

This work presents GPROF-NN XPR, a novel precipitation retrieval designed to overcome limitations of current global PMW precipitation estimates imposed by the shortcomings of the precipitation estimates used as targets for empirical retrieval algorithms. GPROF-NN XPR retrieval combines dedicated estimates of light precipitation based on reference data from the CloudSat CPR with moderate-to-light precipitation estimates based on reference data from the GPM DPR. A simple fusion scheme is proposed to combine the two precipitation estimates into a single fused precipitation estimate. This novel approach extends previous efforts aiming to use CloudSat precipitation rates to retrieve light and frozen precipitation from PMW sensors (Rahimi et al. 2025; Eastman et al. 2019).

Validation of the fused GPROF-NN XPR precipitation estimates shows improved precipitation detection and a reduction of the systematic underestimation that affects conventional retrievals, particularly at high latitudes and for frozen precipitation. These results indicate that GMI PMW

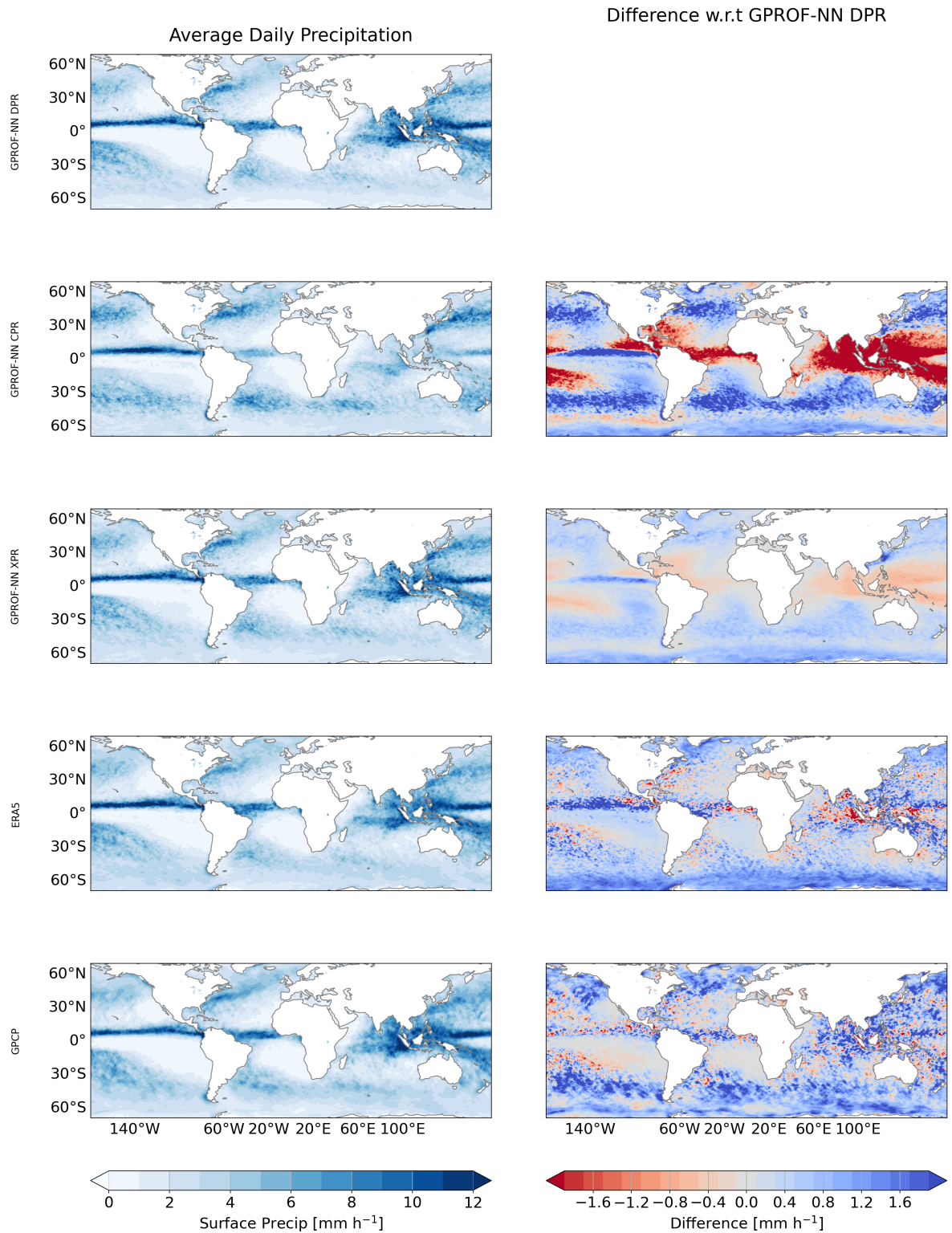


FIG. 15. Global distributions of mean daily precipitation accumulations from the DPR-based estimates (GPROF-NN DPR), the CPR-based estimates (GPROF-NN CPR), and the merged estimates (GPROF-NN XPR) and the ERA5 and GPCP datasets.

observations can help bridge the current sensitivity gap between radar-based precipitation measurements from the CloudSat and GPM missions. By providing estimates that better represent precipitation across regimes, the GPROF-NN XPR retrieval has the potential to improve global precipitation datasets. In particular, it may reduce the need for climatological corrections that suppress monthly and interannual variability.

The improved representation of precipitation across precipitation regimes in the PMW retrievals, also demonstrates that there is potential to improve synergistic active–passive precipitation retrievals using GMI observations. The DPR-based estimates used here are derived from the GPM 2BCMB product, which already combines radar and GMI observations. However, the current algorithm only retrieves precipitation where the radar observations indicate hydrometeor backscatter, which limits the retrievals to the low sensitivity of the DPR. The results presented here demonstrate that GMI observations alone can identify precipitation that is not detected by the DPR, suggesting that current combined radar–radiometer retrievals do not yet fully exploit the synergistic potential of the active and passive microwave observations provided by the GPM satellite.

Although the fused precipitation estimates improve detection and reduce climatological biases, the fusion increases random retrieval errors compared to the DPR-based estimates. Validation of the CPR-based precipitation estimates from the 2C-Rain-Profile product provide more sensitive but generally less accurate quantitative precipitation estimates than the DPR-based reference. The comparison against both ground-based radar and against DPR show large spread at light precipitation rates with a bi-modal tendency to either strongly underestimate or overestimate precipitation by an order of magnitude. The bi-modal behavior of the 2C-Rain-Profile was already noted in the first publication describing the retrieval (Lebsock and L'Ecuyer 2011) but apparently has not been further investigated since. Since 2C-Rain-Profile estimates are used to calibrate principal global precipitation products including IMERG and GPCP (Behrangi and Song 2020), there is a need to revisit these precipitation estimates and ensure consistency with other radar-based precipitation estimates across the shared range of sensitivity.

Despite the uncertainties in the quantitative precipitation estimates from the CPR, our extensive validation of the GPROF-NN XPR estimates against direct, shipborne measurements demonstrates the benefits of using CPR-based precipitation estimates to improve precipitation detection and the climatological representation of high-latitude and frozen precipitation. The GPROF-NN XPR

retrieval will therefore be used as an auxiliary retrieval to add light precipitation to the DPR-based reference data that will be used to train the retrieval algorithms for the next operational version of the GPM PMW retrieval algorithms.

While the GPROF-NN XPR retrieval constitutes an additional step towards improved global estimates of oceanic precipitation from the GPM mission, this work also highlights remaining challenges of current global precipitation products. Since CPR- and DPR-based are currently used in combination to calibrate global precipitation products, it should be ensured that these products are consistent across the shared sensitivity range of CPR and DPR. Moreover, our results indicate that current synergistic active–passive precipitation retrievals underutilize passive observations and could likely be improved to overcome limitations of current active sensors.

Acknowledgments. The work of SP and CDK was supported by NASA grant 80NSSC22K0604.

The authors thank Mathew Lebsock for valuable feedback on the validation of the CloudSat precipitation estimates.

Data availability statement. The 2BCMB can be downloaded from NASA GPM Science Team (2014–present).

The CloudSat 2C-Precip-Column, 2C-Rain-Column, and 2C-Snow-Column data are available from NASA CloudSat Science Team (2006–present).

The OceanRAIN dataset is available from Klepp et al. (2020).

The MRMS data can be downloaded from Iowa Environmental Mesonet (IEM) (2014–present).

References

Ba, J. L., J. R. Kiros, and G. E. Hinton, 2016: Layer normalization. *arXiv preprint arXiv:1607.06450*.

Behrangi, A., and Y. Song, 2020: A new estimate for oceanic precipitation amount and distribution using complementary precipitation observations from space and comparison with GPCP. *Environ. Res. Lett.*, **15** (12), 124 042, <https://doi.org/10.1088/1748-9326/abc6d1>.

Boukabara, S.-A., and Coauthors, 2011: MiRS: An All-Weather 1DVAR Satellite Data Assimilation and Retrieval System. *IEEE Transactions on Geoscience and Remote Sensing*, **49** (9), 3249–3272, <https://doi.org/10.1109/TGRS.2011.2158438>.

Eastman, R., M. Lebsock, and R. Wood, 2019: Warm rain rates from amsr-e 89-ghz brightness temperatures trained using cloudsat rain-rate observations. *Journal of Atmospheric and Oceanic Technology*, **36** (6), 1033 – 1051, <https://doi.org/10.1175/JTECH-D-18-0185.1>.

Ekelund, R., P. Eriksson, and S. Pfreundschuh, 2020: Using passive and active observations at microwave and sub-millimetre wavelengths to constrain ice particle models. *Atmospheric Measurement Techniques*, **13** (2), 501–520, <https://doi.org/10.5194/amt-13-501-2020>.

Greco, M., W. S. Olson, S. J. Munchak, S. Ringerud, L. Liao, Z. Haddad, B. L. Kelley, and S. F. McLaughlin, 2016: The gpm combined algorithm. *Journal of Atmospheric and Oceanic Technology*, **33** (10), 2225–2245.

- Haynes, J. M., T. S. L'Ecuyer, G. L. Stephens, S. D. Miller, C. Mitrescu, N. B. Wood, and S. Tanelli, 2009: Rainfall retrieval over the ocean with spaceborne w-band radar. *Journal of Geophysical Research: Atmospheres*, **114 (D8)**, <https://doi.org/https://doi.org/10.1029/2008JD009973>, <https://agupubs.onlinelibrary.wiley.com/doi/pdf/10.1029/2008JD009973>.
- Hendrycks, D., and K. Gimpel, 2016: Gaussian error linear units (gelus). *arXiv preprint arXiv:1606.08415*.
- Hersbach, H., and Coauthors, 2020: The ERA5 global reanalysis. *Quarterly Journal of the Royal Meteorological Society*, **146 (730)**, 1999–2049, <https://doi.org/10.1002/qj.3803>.
- Huffman, G. J., R. F. Adler, A. Behrangi, D. T. Bolvin, E. J. Nelkin, G. Gu, and M. R. Ehsani, 2023: The New Version 3.2 Global Precipitation Climatology Project (GPCP) Monthly and Daily Precipitation Products. *Journal of Climate*, **36 (21)**, 7635–7655, <https://doi.org/10.1175/JCLI-D-23-0123.1>.
- Huffman, G. J., and Coauthors, 2020: Integrated Multi-satellite Retrievals for the Global Precipitation Measurement (GPM) Mission (IMERG). *Satellite Precipitation Measurement: Volume 1*, V. Levizzani, C. Kidd, D. B. Kirschbaum, C. D. Kummerow, K. Nakamura, and F. J. Turk, Eds., Springer International Publishing, Cham, 343–353, https://doi.org/10.1007/978-3-030-24568-9_19, URL https://doi.org/10.1007/978-3-030-24568-9_19.
- Iowa Environmental Mesonet (IEM), 2014–present: Multi-Radar Multi-Sensor (MRMS) Data Archive. Iowa State University, accessed: 2026-04-08, <https://mtarchive.geol.iastate.edu/>.
- Kidd, C., and G. Huffman, 2011: Global precipitation measurement. *Meteorological Applications*, **18 (3)**, 334–353, <https://doi.org/10.1002/met.284>.
- Klepp, C., and Coauthors, 2018: Oceanrain, a new in-situ shipboard global ocean surface-reference dataset of all water cycle components. *Scientific Data*, **5 (1)**, 180 122.
- Klepp, C., and Coauthors, 2020: OceanRAIN Release 2.0 (Ocean Rainfall And Ice-phase precipitation measurement Network). Deutscher Wetterdienst (DWD), Climate Data Center (CDC), version 2.0, Accessed: 2026-04-08, https://opendata.dwd.de/climate_environment/CDC/help/landing_pages/doi_landingpage_OceanRAIN_V002-en.html.

- Kummerow, C. D., D. L. Randel, M. Kulie, N.-Y. Wang, R. Ferraro, S. J. Munchak, and V. Petkovic, 2015: The Evolution of the Goddard Profiling Algorithm to a Fully Parametric Scheme. *Journal of Atmospheric and Oceanic Technology*, **32** (12), 2265–2280, <https://doi.org/10.1175/JTECH-D-15-0039.1>.
- Lebsock, M. D., and T. S. L'Ecuyer, 2011: The retrieval of warm rain from cloudsat. *Journal of Geophysical Research: Atmospheres*, **116** (D20), <https://doi.org/https://doi.org/10.1029/2011JD016076>, <https://agupubs.onlinelibrary.wiley.com/doi/pdf/10.1029/2011JD016076>.
- Liu, Z., H. Mao, C.-Y. Wu, C. Feichtenhofer, T. Darrell, and S. Xie, 2022: A convnet for the 2020s. *Proceedings of the IEEE/CVF conference on computer vision and pattern recognition*, 11 976–11 986.
- Milani, L., and C. Kidd, 2023: The State of Precipitation Measurements at Mid-to-High Latitudes. *Atmosphere*, **14** (11), 1677, <https://doi.org/10.3390/atmos14111677>.
- NASA CloudSat Science Team, 2006–present: CloudSat Data Processing Center (DPC). Colorado State University / NASA Jet Propulsion Laboratory, accessed: 2026-04-08, <https://www.cloudsat.cira.colostate.edu/>.
- NASA GPM Science Team, 2014–present: GPM DPR/GMI Combined Radar-Radiometer (2BCMB) Level-2 Data. NASA Goddard Earth Sciences Data and Information Services Center (GES DISC), accessed: 2026-04-08, https://disc.gsfc.nasa.gov/datasets/GPM_2BCMB_07/summary.
- Pfreundschuh, S., P. J. Brown, C. D. Kummerow, P. Eriksson, and T. Norrestad, 2022: GPROF-NN: a neural-network-based implementation of the Goddard Profiling Algorithm. *Atmospheric Measurement Techniques*, **15** (17), 5033–5060, <https://doi.org/10.5194/amt-15-5033-2022>.
- Pfreundschuh, S., P. Eriksson, D. Duncan, B. Rydberg, N. Håkansson, and A. Thoss, 2018: A neural network approach to estimating a posteriori distributions of Bayesian retrieval problems. *Atmospheric Measurement Techniques*, **11** (8), 4627–4643, <https://doi.org/10.5194/amt-11-4627-2018>.
- Pfreundschuh, S., C. Guilloteau, P. J. Brown, C. D. Kummerow, and P. Eriksson, 2024: GPROF V7 and beyond: assessment of current and potential future versions of the GPROF passive

- microwave precipitation retrievals against ground radar measurements over the continental US and the Pacific Ocean. *Atmospheric Measurement Techniques*, **17 (2)**, 515–538, <https://doi.org/10.5194/amt-17-515-2024>.
- Pfreundschuh, S., and Coauthors, 2026: A benchmark dataset for satellite-based estimation and detection of rain. *Scientific Data*.
- Rahimi, R., A. Ebtehaj, and L. Milani, 2025: Advancing passive microwave retrievals of precipitation using cloudsat and gpm coincidences: Integration of machine learning with a bayesian algorithm. *Journal of Hydrometeorology*, **26 (5)**, 537–553.
- Sims, E. M., and G. Liu, 2015: A parameterization of the probability of snow–rain transition. *Journal of hydrometeorology*, **16 (4)**, 1466–1477.
- Smith, T. M., and Coauthors, 2016: Multi-Radar Multi-Sensor (MRMS) Severe Weather and Aviation Products: Initial Operating Capabilities. *Bulletin of the American Meteorological Society*, **97 (9)**, 1617–1630, <https://doi.org/10.1175/BAMS-D-14-00173.1>.
- Stephens, G. L., and Coauthors, 2008: Cloudsat mission: Performance and early science after the first year of operation. *Journal of Geophysical Research: Atmospheres*, **113 (D8)**.
- Tan, M., and Q. Le, 2021: Efficientnetv2: Smaller models and faster training. *International conference on machine learning*, PMLR, 10 096–10 106.
- Wood, N. B., T. S. L'Ecuyer, A. J. Heymsfield, G. L. Stephens, D. R. Hudak, and P. Rodriguez, 2014: Estimating snow microphysical properties using collocated multisensor observations. *Journal of Geophysical Research: Atmospheres*, **119 (14)**, 8941–8961, <https://doi.org/https://doi.org/10.1002/2013JD021303>, <https://agupubs.onlinelibrary.wiley.com/doi/pdf/10.1002/2013JD021303>.